




Engineering Notes

Equinoctial Lyapunov Control Law for Low-Thrust Rendezvous

Sanjeev Narayanaswamy*[✉] and Christopher J. Damaren[†] 
University of Toronto, Toronto, Ontario M3H 5T6, Canada

<https://doi.org/10.2514/1.G006662>

I. Introduction

SPACE rendezvous occurs when two or more objects in space are brought together for station-keeping or docking. This is characterized by a small relative displacement and, to avoid a collision, a small relative velocity. For conventional engines, simple impulsive maneuvers exist that can be used in the preliminary design stage to model the various orbital element changes required to achieve rendezvous [1]. Preliminary design for low-thrust rendezvous trajectories using ion thrusters is less straightforward. In spite of the challenges, low-thrust rendezvous can enable significant fuel savings due to the use of engines with high specific impulses. Some promising geocentric applications of low-thrust rendezvous include orbital debris removal [2] and spacecraft servicing [3].

Several approaches to low-thrust rendezvous trajectory design exist. Linearized assumptions leading to equation sets such as the famous Hill–Clohessy–Wiltshire (HCW) equations can be used for short-range low-thrust rendezvous [4–7]. Another approach, based on the calculus of variations, is known as the indirect method [8,9]. Because this approach is quite sensitive to the initial guess, the homotopy method is sometimes used as a way of generating a series of progressively better initial guesses [10]. One popular and straightforward method for interplanetary rendezvous optimization is the Sims–Flanagan method [11,12]. It approximates a low-thrust trajectory as a series of small impulsive thrusts, which are then optimized. Shape-based methods provide a good initial guess for direct methods because they involve sets of parameters that analytically describe families of trajectories that satisfy the equations of motion [13–16]. A drawback of this approach is that the trajectories are often limited to a small number of revolutions.

Low-thrust rendezvous design for geocentric orbits has a different set of difficulties when compared to interplanetary rendezvous design. The main difficulty is due to the larger number of revolutions required and the fact that the target and chaser spacecraft are no longer in the vicinity of a single plane—the ecliptic. The Sims–Flanagan method becomes computationally intractable for a general three-dimensional rendezvous in a geocentric orbit due to the fine mesh needed to accurately represent the faster dynamics about the primary gravitational body. Other direct methods, such as pseudospectral methods [17], that rely on more computationally

efficient methods of discretization, can be used as long as a suitable initial guess is chosen [18].

The use of Lyapunov feedback control laws for low-thrust space orbit transfers is an interesting area of research that can be adapted for rendezvous. These laws are similar to the thrust-blending laws, such as those by Kluever [19] and Ruggiero et al. [20], which seek to instantaneously blend the thrust profiles that maximize the rate of change of the orbital elements through tunable weights, rather than by using a Lyapunov function. First introduced by Ilgen [21] in 1993 for orbital transfers, Lyapunov control laws instead rely on steering a spacecraft such that the error between the current orbit and the desired orbit is driven to zero by making the rate of change of an appropriately chosen scalar Lyapunov function as negative as possible [22]. Although suboptimal, Lyapunov feedback control laws can produce trajectories that are close to optimal, depending on the chosen parameters [23,24]. Alternatively, they can be used to provide a good initial guess for direct methods [25]. Naasz [26] developed three Lyapunov control laws using constant gains for Cartesian coordinates, classical elements, and equinoctial elements. In his control law based on classical orbital elements, Naasz also provided a mechanism for targeting the fast variable so that static six-state targeting is achieved. For the planar low-thrust rendezvous problem, Hernandez and Akella [27] have applied a Lyapunov control law using Levi–Cevita coordinates. The work by Leomanni et al. [28] presented a modified equinoctial element Lyapunov feedback control law for tracking true longitude in addition to the other orbital elements in order to attain dynamic rendezvous targeting.

Over a series of papers starting in 2003, and refined in 2005, Petropoulos developed a sophisticated Lyapunov-based control law named the Q-Law [23,29,30] for low-thrust orbital transfers. It uses a candidate Lyapunov function, Q , that is related to the square of the minimum time required to reach the target orbit. An important aspect of this control law is the way the function Q encapsulates the connections between the rates of change of the various orbital elements while also including built-in mechanisms for coasting to save fuel and for remaining above a minimum periapsis radius. The Q-Law in its original form was stated using classical elements, but versions using the modified equinoctial elements have been developed in order to avoid the associated singularities. Notable examples include the work by Joseph [31], who applied equinoctial elements to a simplified version of the Q-Law and used proportional–integral control in order to control the ground track angle for stationkeeping. An interesting application of the Q-Law for solar sail trajectories is the work by Niccolai et al. [32], where various heliocentric mission scenarios were investigated. Varga and Pérez [24] were the first to approach the refined formulation of the Q-Law from an equinoctial framework. Lantukh et al. [33] then augmented Petropoulos' classical element version of the Q-Law with an improved version of Naasz's fast variable targeting mechanism to produce the Enhanced Q-Law (EQ-Law) with six-state targeting capability. However, this only transfers the spacecraft to a certain stationary point in space. In that study, it was stated that it would be interesting to investigate the use of a Q-Law for achieving rendezvous with a moving target [33].

In the present work, the best aspects of the existing Lyapunov control laws discussed in the previous paragraphs have been combined and modified to create a Rendezvous Q-Law (RQ-Law) that is capable of targeting a time-varying point in space. We started with the Q-Law formed by Varga and Pérez [24] as it uses modified equinoctial elements with Petropoulos's refined form of the Lyapunov function [23]. We then modified this control law to provide a more accurate calculation of the thruster firing angles. Then to enable dynamic rendezvous targeting, we developed a novel target semimajor axis augmentation scheme. A comparison of the RQ-Law with other Lyapunov control laws for low-thrust trajectories is given in Table 1. It is seen that the properties of the RQ-Law address the existing

Received 4 January 2022; revision received 29 June 2022; accepted for publication 11 January 2023; published online 24 February 2023. Copyright © 2023 by Sanjeev Narayanaswamy and Christopher J. Damaren. Published by the American Institute of Aeronautics and Astronautics, Inc., with permission. All requests for copying and permission to reprint should be submitted to CCC at www.copyright.com; employ the eISSN 1533-3884 to initiate your request. See also AIAA Rights and Permissions www.aiaa.org/randp.

*Ph.D. Candidate, Spacecraft Dynamics and Control Laboratory, Institute for Aerospace Studies, 4925 Dufferin Street; sanjeev.narayanaswamy@mail.utoronto.ca. Student Member AIAA.

[†]Professor and Director, Institute for Aerospace Studies, 4925 Dufferin Street; damaren@utias.utoronto.ca. Associate Fellow AIAA.

Table 1 Comparison of the RQ-Law with other selected low-thrust Lyapunov feedback control laws

Lyapunov control law	Based on Petropoulos Q-Law	Orbital element set	Orbit targeting	Static six-element targeting	Dynamic rendezvous targeting	Other notes
Ilggen (1993) [21]	—	Classical and modified equinoctial	✓	—	—	Introduced the use of a Lyapunov function for low-thrust orbit transfers
Chang et al. (2002) [34]	—	—	✓	—	—	Introduced the use of a Lyapunov function based on the eccentricity and angular momentum vectors
Naasz (2002) [26]	—	Classical	✓	✓	—	Introduced the concept of mean motion control for targeting a particular phase angle through a classical Lyapunov control law—while two other Lyapunov control laws based on Cartesian and equinoctial frameworks were given in this work, those laws did not use mean motion control
Petropoulos Q-Law (2005) [23]	✓	Classical	✓	—	—	Reference formulation of the refined Q-Law
Varga and Pérez Q-Law (2016) [24]	✓	Modified equinoctial	✓	—	—	Introduced the use of modified equinoctial elements for the refined version of the Q-Law
Leomanni et al. (2016) [28]	—	Modified equinoctial	✓	✓	✓	Introduced dynamic rendezvous targeting for a Lyapunov control law
Lantukh et al. EQ-Law (2017) [33]	✓	Classical	✓	✓	—	Introduced static six-element targeting for the refined Q-Law
RQ-Law	✓	Modified equinoctial	✓	✓	✓	Introduces dynamic rendezvous targeting for the refined Q-Law with a more accurate method of thrust angle determination and a novel target semimajor axis augmentation scheme that accounts for a minimum periapsis constraint

research gap for a Q-Law variant that is capable of dynamic rendezvous.

The structure of the remainder of this work will be as follows. The RQ-Law and the necessary background will be described in Sec. II. In Sec. III this law will be demonstrated with numerical examples, including several cases where comparisons are given with existing control laws. Finally, in Sec. IV, the RQ-Law and the presented analysis will be summarized.

II. Space Rendezvous Using a Lyapunov Control Law Based on Modified Equinoctial Elements

A. Modified Equinoctial Elements

The conversion from the set of classical elements (a [m] semimajor axis, e eccentricity, i [rad] inclination, ω [rad] argument of periapsis, Ω [rad] right ascension of the ascending node (RAAN), θ [rad] true anomaly) to the set of modified equinoctial elements (p [m] semilatus rectum, f, g, h, k, L [rad] true longitude), as defined by Walker et al. [35], is given by

$$p = a(1 - e^2) \quad (1)$$

$$\alpha_{T,\text{aug}} = \begin{cases} \frac{2W_L}{\pi} \left(a_T - \frac{r_{p,\text{min}}}{1 - \sqrt{f_C^2 + g_C^2}} \right) \tan^{-1}(W_{\text{sc1}} \Delta L_{[-\pi,\pi]}) + a_T, & \alpha = a \\ \alpha_T, & \alpha \in \{f, g, h, k\} \end{cases} \quad (8)$$

$$f = e \cos(\omega + \Omega) \quad (2)$$

$$g = e \sin(\omega + \Omega) \quad (3)$$

$$h = \tan(i/2) \cos(\Omega) \quad (4)$$

$$k = \tan(i/2) \sin(\Omega) \quad (5)$$

$$L = \theta + \omega + \Omega \quad (6)$$

B. RQ-Law Description

The Lyapunov function that we will use takes the form

$$Q = (1 + W_p P) \sum_{\alpha} S_{\alpha} W_{\alpha} \left(\frac{\alpha_C - \alpha_{T,\text{aug}}}{\dot{\alpha}_{C,\text{max},\alpha\beta L}} \right)^2, \quad \alpha \in \{a, f, g, h, k\} \quad (7)$$

where we note that the semimajor axis a is used instead of the semilatus rectum, p , in the set of modified equinoctial elements, α , because this was the approach taken by both Naasz [26] and Varga and Pérez [24]. It was found by Varga and Pérez that this substitution results in a better controller performance than if the original set of modified equinoctial elements is used [24]. It is also noted that Q has units of time squared. As will be discussed later in this paper, the quantity P is the penalty function, W_p is the associated weight, and S_{α} is the scaling function. The set α_C corresponds to the orbital elements of the chaser, W_{α} are the associated scalar weights, and the augmented set of target orbital elements, $\alpha_{T,\text{aug}}$, is defined as

where the set α_T represents the unaugmented target orbital elements. The quantity $\Delta L_{[-\pi,\pi]} = L_C - L_T$, is the difference in radians between the true longitudes of the chaser and target wrapped to the range $[-\pi, \pi]$, $r_{p,\text{min}}$ is the minimum periapsis radius constraint, and W_L and W_{sc1} are phasing parameters. Canonical units are used with a suitable distance scaling unit, DU , and a time scaling unit, TU , in the description and implementation of the RQ-Law, such that the scaled standard gravitational parameter is unity.

To perform phasing, the augmented form of $a_{T,\text{aug}}$ in Eq. (8) has been designed to induce an error in the semimajor axis that is related

to the amount of error in the true longitude. The semimajor axis augmentation scheme is constructed around the arctangent function, because it offers known upper and lower bounds that are controllable through the parameter W_L and a simple derivative that is controllable through the W_{sc1} parameter. If $\Delta L_{[-\pi,\pi]} > 0$, then $a_{T,aug} > a_T$, and if $\Delta L_{[-\pi,\pi]} < 0$, then $a_{T,aug} < a_T$. This enables the final convergence of the phase angle through the shorter way around the orbit. A plot of this target semimajor axis augmentation scheme is shown in Fig. 1, as a function of ΔL . We note that the upper and lower bounds of $a_{T,aug}$ are asymptotic and deviate from a_T by

$$\pm W_L \left(a_T - \frac{r_{p,min}}{1 - \sqrt{f_C^2 + g_C^2}} \right)$$

In addition, the relation between the radius of periapsis, r_p , and the semimajor axis is known [1] to be $a = r_p/(1 - e) = r_p/(1 - \sqrt{f^2 + g^2})$. Therefore with this scheme, as long as $0 \leq W_L \leq 1$, this will prevent the r_p corresponding to the lower bound of $a_{T,aug}$,

$$a_T - W_L \left(a_T - \frac{r_{p,min}}{1 - \sqrt{f_C^2 + g_C^2}} \right)$$

from being below the minimum periapsis radius constraint, $r_{p,min}$. We also note that in Fig. 1, a semimajor axis value of $1/(1 - \sqrt{f_C^2 + g_C^2})$ corresponds to an r_p of one distance scaling unit (1 DU). If DU is chosen to be the radius of the primary gravitational body, such as the radius of the Earth, and if $r_{p,min} > 1$ and $0 \leq W_L \leq 1$, this scheme can ensure that a collision of the chaser with the surface of the primary does not occur during target acquisition. By varying the phasing parameters W_L and W_{sc1} , the maximum deviation and rate of change of the augmented target semimajor axis, $a_{T,aug}$, with respect to the true longitude error, $\Delta L_{[-\pi,\pi]}$, can be controlled. When compared to Lantukh's [33] semimajor axis augmentation scheme, it is apparent that the approach taken by the RQ-Law does not require the N_{tr} , time-to-go concept, which is an estimate of the remaining number of revolutions to reach the target. As will be explained in more detail in Sec. III, this is because the RQ-Law splits a trajectory into two stages, and phasing is started only after the errors in the slow elements have been driven close to zero.

The quantity $\dot{a}_{C,max,\alpha\beta L}$ represents the maximum rate of change for each chaser orbital element, α_C , with respect to both thrust direction and true longitude. The following expressions, $\dot{a}_{max,\alpha\beta L}$, expressed in

modified equinoctial elements for any maneuvering spacecraft, can be obtained from Varga and Pérez [24]:

$$\dot{a}_{max,\alpha\beta L} = 2Fa \sqrt{\frac{a}{\mu}} \sqrt{\frac{1 + \sqrt{f^2 + g^2}}{1 - \sqrt{f^2 + g^2}}} \quad (9)$$

$$\dot{f}_{max,\alpha\beta L} \approx 2F \sqrt{\frac{a(1 - f^2 - g^2)}{\mu}} \quad (10)$$

$$\dot{g}_{max,\alpha\beta L} \approx 2F \sqrt{\frac{a(1 - f^2 - g^2)}{\mu}} \quad (11)$$

$$\dot{h}_{max,\alpha\beta L} = \frac{1}{2}F \sqrt{\frac{a(1 - f^2 - g^2)}{\mu}} \frac{s^2}{\sqrt{1 - g^2 + f}} \quad (12)$$

$$\dot{k}_{max,\alpha\beta L} = \frac{1}{2}F \sqrt{\frac{a(1 - f^2 - g^2)}{\mu}} \frac{s^2}{\sqrt{1 - f^2 + g}} \quad (13)$$

where the given expressions for $\dot{f}_{max,\alpha\beta L}$ and $\dot{g}_{max,\alpha\beta L}$ are approximations, $s^2 = 1 + h^2 + k^2$, and F is the magnitude of the propulsive acceleration $\mathbf{F} = \mathbf{T}/m$. The thrust magnitude, T , can be related [36] to the engine efficiency (η_{eng}), engine power (P_{eng}), specific impulse (I_{sp}), standard gravity (g_0), and mass flow rate (\dot{m}), using $T = (2\eta_{eng}P_{eng})/(g_0I_{sp}) = I_{sp}\dot{m}g_0$. However, as will be explained in Sec. II.B.1, the approximations for $\dot{f}_{max,\alpha\beta L}$ and $\dot{g}_{max,\alpha\beta L}$ given in Eqs. (10) and (11) are inaccurate for certain orbits. Therefore, an alternate method of characterizing $\dot{f}_{max,\alpha\beta L}$ and $\dot{g}_{max,\alpha\beta L}$ is developed, which is used in the RQ-Law.

The penalty function, P , is given by

$$P = \exp \left[k_{pen} \left(1 - \frac{r_{p,C}}{r_{p,min}} \right) \right] \quad (14)$$

and this helps to make the minimum radius of the chaser spacecraft, $r_{p,C} = a_C(1 - e_C)$, stay above a specified $r_{p,min}$. The scalar k_{pen} and, as mentioned earlier, W_p are weights associated with this penalty function. Here we note that the lower bound of the semimajor axis augmentation scheme in Eq. (8) has been designed to avoid interfering with the functionality of the penalty function. The scaling function S_{α} can be written as

$$S_{\alpha} = \begin{cases} \left[1 + \left(\frac{|a_C - a_{T,aug}|}{m_{sc1}a_{T,aug}} \right)^{n_{sc1}} \right]^{1/r_{sc1}}, & \alpha = a \\ 1, & \alpha \in \{f, g, h, k\} \end{cases} \quad (15)$$

where the quantities m_{sc1} , n_{sc1} , and r_{sc1} are associated scalar weights. Since $\dot{a}_{max,\alpha\beta L}$ in Eqs. (9–13), become infinite as $a \rightarrow \infty$, the value of Q can be reduced to zero when $a_C \rightarrow \infty$ in addition to the desired behavior of $a_C \rightarrow a_{T,aug}$ [24]. The expression for S_a prevents a_C from approaching infinity [23].

For a spacecraft equipped with a constant-thrust engine, the in-plane and out-of-plane Lyapunov-optimal thrust angles, α^* and β^* , need to be found such that whenever the thrusters are on, \dot{Q} is minimized. The thrust angles are defined in the local-vertical-local-horizontal (LVLH) frame

$$\mathcal{F}_{LVLH} = \begin{bmatrix} \mathbf{r} & \mathbf{h} \times \mathbf{r} & \mathbf{h} \\ |\mathbf{r}| & |\mathbf{h} \times \mathbf{r}| & |\mathbf{h}| \end{bmatrix}^T$$

attached to the chaser spacecraft. The propulsive acceleration \mathbf{F} is related to the thrust angles α and β via

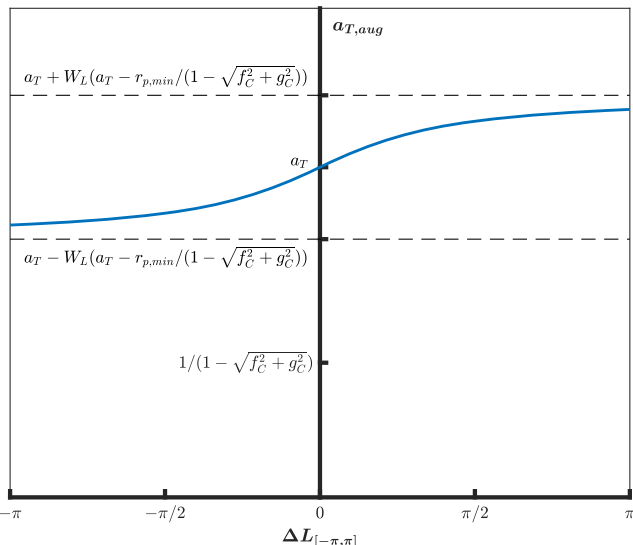


Fig. 1 A plot showing the behavior of the augmented target semimajor axis $a_{T,aug}$, in nondimensionalized units DU, with respect to the difference in true longitude, $\Delta L_{[-\pi,\pi]}$, in radians.

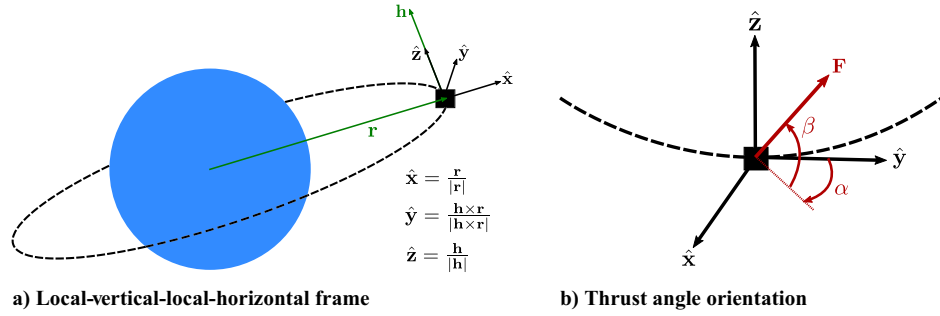


Fig. 2 Description of the LVLH frame and the thrust angle orientation.

$$\mathbf{F} = \begin{bmatrix} F_r \\ F_\theta \\ F_h \end{bmatrix} = \begin{bmatrix} F \cos \beta \sin \alpha \\ F \cos \beta \cos \alpha \\ F \sin \beta \end{bmatrix} \quad (16)$$

Diagrams of the LVLH frame and the geometry of the thrust angles are shown in Fig. 2. The expressions for the Lyapunov-optimal thrust angles, α^* and β^* , are derived in Sec. II.B.1.

Numerical propagation of the nonlinear dynamics of a spacecraft using modified equinoctial elements can be done using Gauss' variational equations [24]:

$$\begin{bmatrix} \dot{a} \\ \dot{f} \\ \dot{g} \\ \dot{h} \\ \dot{k} \\ \dot{L} \end{bmatrix} = \mathbf{A} \begin{bmatrix} F_r \\ F_\theta \\ F_h \end{bmatrix} + \mathbf{b} \quad (17)$$

where the matrix \mathbf{A} and column vector \mathbf{b} are expressed as

$$\mathbf{A} = \frac{1}{q} \sqrt{\frac{a(1-f^2-g^2)}{\mu}} \begin{bmatrix} \frac{2aq(f \sin(L)-g \cos(L))}{1-f^2-g^2} & \frac{2aq^2}{1-f^2-g^2} & 0 \\ q \sin(L) & (q+1) \cos(L) + f & -g(h \sin(L) - k \cos(L)) \\ -q \cos(L) & (q+1) \sin(L) + g & f(h \sin(L) - k \cos(L)) \\ 0 & 0 & \frac{\cos(L)}{2}(1+h^2+k^2) \\ 0 & 0 & \frac{\sin(L)}{2}(1+h^2+k^2) \\ 0 & 0 & h \sin(L) - k \cos(L) \end{bmatrix} \quad (18)$$

$$\mathbf{b} = \begin{bmatrix} 0 & 0 & 0 & 0 & 0 & \frac{q^2 \sqrt{a\mu(1-f^2-g^2)}}{a^2(1-f^2-g^2)^2} \end{bmatrix}^T \quad (19)$$

with

$$q = 1 + f \cos(L) + g \sin(L) \quad (20)$$

For the RQ-Law, we note that the target is propagated from its initial conditions without control and that the mass history of the chaser is calculated using the rocket equation. This means that the acceleration due to thrust increases as the spacecraft mass decreases. The algorithm is terminated when the desired rendezvous tolerances are met.

We also adopt the notion of relative effectivity, η_r , to create a coasting mechanism [23]. This is defined as $\eta_r = (\dot{Q}_n - \dot{Q}_{nx} / \dot{Q}_{nn} - \dot{Q}_{nx})$,

where \dot{Q}_n is the Lyapunov-optimal value of \dot{Q} at the current time t and

$$\dot{Q}_{nn} = \min_{[t, t+T]} \dot{Q}_n \quad (21)$$

$$\dot{Q}_{nx} = \max_{[t, t+T]} \dot{Q}_n \quad (22)$$

The quantities \dot{Q}_{nn} and \dot{Q}_{nx} represent the minimum and maximum values of \dot{Q}_n that could occur in the current osculating orbit of the chaser. Because we simultaneously propagate the target for rendezvous, we have chosen to evaluate η_r at each time step by using a temporal mesh defined as $[t, t+T]$, where t is the current time step and T is the period of the current osculating orbit of the chaser. This is in contrast to a previous study that used a phase angle mesh to evaluate the relative effectivity at each time step for an orbital transfer problem [25]. If $\eta_r \geq \eta_{r, \text{tol}}$, where $\eta_{r, \text{tol}}$ is some set tolerance value, then the propulsion system for the chaser is turned on. Otherwise, the spacecraft is allowed to coast, trading a higher time of flight for lower fuel consumption.

1. Lyapunov-Optimal Thrust Angles from Combined Analytical and Numerical Partial Derivatives

We decided to find more accurate approximations for the maximal rates of change for the modified equinoctial elements $f = e \cos(\omega + \Omega)$ and $g = e \sin(\omega + \Omega)$ given by Varga and Pérez [24]:

$$\dot{f}_{\max, \alpha\beta L} \approx 2F \sqrt{\frac{p}{\mu}} \quad (23)$$

$$\dot{g}_{\max, \alpha\beta L} \approx 2F \sqrt{\frac{p}{\mu}} \quad (24)$$

The starting point for our analysis was the equations given by Yuan et al. [37]:

$$\dot{f}_{\max, \alpha\beta} = \frac{F}{q} \sqrt{\frac{p}{\mu}} \sqrt{(f + \sin(L)(q+1))^2 + q^2 \sin^2(L) + g^2(k \cos(L) - h \sin(L))^2} \quad (25)$$

$$\dot{g}_{\max, \alpha\beta} = \frac{F}{q} \sqrt{\frac{p}{\mu}} \sqrt{(g + \sin(L)(q+1))^2 + q^2 \cos^2(L) + f^2(k \cos(L) - h \sin(L))^2} \quad (26)$$

where $q = 1 + f \cos(L) + g \sin(L)$, as defined before, and $p = a(1 - f^2 - g^2)$. It should be noted that Eqs. (23) and (24) give the approximate maximal rates of change over the thrust angles and the true longitude L for a particular osculating orbit, while Eqs. (25) and (26) only give the maximal rates of change over the thrust angles.

Here we compare the values of $\dot{f}_{\max,\alpha\beta L}$ and $\dot{g}_{\max,\alpha\beta L}$ found from the maxima of the expressions for $\dot{f}_{\max,\alpha\beta}$ and $\dot{g}_{\max,\alpha\beta}$ given by Yuan et al. [37], with their approximation, $2F\sqrt{(p/\mu)}$, proposed by Varga and Pérez [24]. The behavior of Eqs. (23–26) can be visualized in Fig. 3 where various plots of $\dot{f}_{\max,\alpha\beta} - 2F\sqrt{(p/\mu)}$ and $\dot{g}_{\max,\alpha\beta} - 2F\sqrt{(p/\mu)}$ are shown. The parameters used for these plots are $F = 1, \mu = 1, a = 7.6, \omega = 3.52$ rad, and $\Omega = 1.97$ rad with three different sets of eccentricities and inclinations. We note that for ease of interpretation, classical elements are used to specify the orbits in Fig. 3, but these are converted to modified equinoctial elements internally. It can be seen that, for orbits with a low eccentricity and inclination, the approximation performs well (markers are close to zero), but for orbits that are highly eccentric ($e \approx 0.8$) or have a high inclination ($i \approx 3.1$ rad), the values of $\dot{f}_{\max,\alpha\beta L}$ and $\dot{g}_{\max,\alpha\beta L}$ found using Eqs. (25) and (26) can be much different from the approximations in Eqs. (23) and (24). This indicates that it would be advantageous to base the thrust angle determination on Eqs. (25) and (26) as they can be used to find the correct orbit-dependent values of $\dot{f}_{\max,\alpha\beta L}$ and $\dot{g}_{\max,\alpha\beta L}$. To address this, the approach taken in the RQ-Law is to numerically evaluate $\dot{f}_{\max,\alpha\beta}$ and $\dot{g}_{\max,\alpha\beta}$ at a mesh of various true longitude values, in order to determine $\dot{f}_{\max,\alpha\beta L}$ and $\dot{g}_{\max,\alpha\beta L}$.

which is used to achieve rendezvous. By using Eqs. (17–20), \dot{L} is expressed as

$$\dot{L} = \frac{F_h}{q} \sqrt{\frac{a(1-f^2-g^2)}{\mu}} (h \sin(L) - k \cos(L)) + \frac{q^2 \sqrt{a\mu(1-f^2-g^2)}}{a^2(1-f^2-g^2)^2} \tag{28}$$

$$= A_{(6,3)} F_h + b_6 \tag{29}$$

where $A_{(6,3)}$ represents the element in the A matrix at the given (row, column) index and b_6 represents the sixth element of the b column vector. For the rates of change of the chaser and target true longitudes, this means

$$\dot{L}_C = A_{C,(6,3)} F_h + b_{C,6} \tag{30}$$

$$\dot{L}_T = A_{T,(6,3)} F_h^0 + b_{T,6} \tag{31}$$

$$= b_{T,6} \tag{32}$$

where F_h is zero in the expression for \dot{L}_T because the target is uncontrolled. Therefore, \dot{Q} can be written using the chain rule as

$$\dot{Q} = \sum_{\alpha} \left(\frac{\partial Q}{\partial \alpha_C} \dot{\alpha}_C + \frac{\partial Q}{\partial \alpha_T} \dot{\alpha}_T^0 + \frac{\partial Q}{\partial \dot{f}_{C,\max,\alpha\beta L}} \frac{\partial \dot{f}_{C,\max,\alpha\beta L}}{\partial \alpha_C} \dot{\alpha}_C + \frac{\partial Q}{\partial \dot{g}_{C,\max,\alpha\beta L}} \frac{\partial \dot{g}_{C,\max,\alpha\beta L}}{\partial \alpha_C} \dot{\alpha}_C \right) + \frac{\partial Q}{\partial \psi} \dot{\psi}^0 + \frac{\partial Q}{\partial L_C} \dot{L}_C + \frac{\partial Q}{\partial L_T} \dot{L}_T \tag{33}$$

$$= \sum_{\alpha} \left(\frac{\partial Q}{\partial \alpha_C} \dot{\alpha}_C + \frac{\partial Q}{\partial \dot{f}_{C,\max,\alpha\beta L}} \frac{\partial \dot{f}_{C,\max,\alpha\beta L}}{\partial \alpha_C} \dot{\alpha}_C + \frac{\partial Q}{\partial \dot{g}_{C,\max,\alpha\beta L}} \frac{\partial \dot{g}_{C,\max,\alpha\beta L}}{\partial \alpha_C} \dot{\alpha}_C \right) + \frac{\partial Q}{\partial L_C} \dot{L}_C + \frac{\partial Q}{\partial L_T} \dot{L}_T \tag{34}$$

$$= \sum_{\alpha} \left(\frac{\partial Q}{\partial \alpha_C} + \frac{\partial Q}{\partial \dot{f}_{C,\max,\alpha\beta L}} \frac{\partial \dot{f}_{C,\max,\alpha\beta L}}{\partial \alpha_C} + \frac{\partial Q}{\partial \dot{g}_{C,\max,\alpha\beta L}} \frac{\partial \dot{g}_{C,\max,\alpha\beta L}}{\partial \alpha_C} \right) \dot{\alpha}_C + \frac{\partial Q}{\partial L_C} (A_{C,(6,3)} F_h + b_{C,6}) + \frac{\partial Q}{\partial L_T} (b_{T,6}) \tag{35}$$

The Lyapunov function Q is a function of several quantities: the chaser and target orbital elements, the chaser and target true longitudes, L_C and L_T , as well as a set of constants $\psi = \{W_p, W_a, W_f, W_g, W_h, W_k, W_L, W_{scl}, k_{pen}, m_{scl}, \mu, n_{scl}, r_{scl}, r_{p,min}\}$. So the dependence of Q on these quantities can be expressed as

$$Q(\alpha_C, \alpha_T, L_C, L_T, \psi) \tag{27}$$

It is important to note that the dependence of Q on L_C and L_T is due to their presence in Eq. (8) for the augmented target semimajor axis,

where $\dot{\alpha}_T$ is zero because the target is uncontrolled, and $\dot{\psi}$ is zero because ψ is composed of constants. We note that in Eqs. (33–35), although the analytical expressions of $\dot{f}_{C,\max,\alpha\beta L}$ and $\dot{g}_{C,\max,\alpha\beta L}$ are unknown, they are functions of α_C , as can be seen from the expressions for $\dot{f}_{\max,\alpha\beta}$ and $\dot{g}_{\max,\alpha\beta}$ in Eqs. (25) and (26). For this reason, we use the chain rule to reveal their dependence on α_C through the partial derivatives $\partial \dot{f}_{C,\max,\alpha\beta L} / \partial \alpha_C$ and $\partial \dot{g}_{C,\max,\alpha\beta L} / \partial \alpha_C$. After expanding $\dot{\alpha}_C$ in terms of the propulsive acceleration components, we can express these components in terms of the thrust angles:

$$\begin{aligned} \dot{Q} = & \sum_{\alpha} \left(\frac{\partial Q}{\partial \alpha_C} + \frac{\partial Q}{\partial \dot{f}_{C,\max,\alpha\beta L}} \frac{\partial \dot{f}_{C,\max,\alpha\beta L}}{\partial \alpha_C} + \frac{\partial Q}{\partial \dot{g}_{C,\max,\alpha\beta L}} \frac{\partial \dot{g}_{C,\max,\alpha\beta L}}{\partial \alpha_C} \right) \\ & \cdot \left(\frac{\partial \dot{\alpha}_C}{\partial F_{\theta}} F \cos \beta \cos \alpha + \frac{\partial \dot{\alpha}_C}{\partial F_r} F \cos \beta \sin \alpha + \frac{\partial \dot{\alpha}_C}{\partial F_h} F \sin \beta \right) \\ & + \frac{\partial Q}{\partial L_C} (A_{C,(6,3)} F_h + b_{C,6}) + \frac{\partial Q}{\partial L_T} (b_{T,6}) \end{aligned} \tag{36}$$

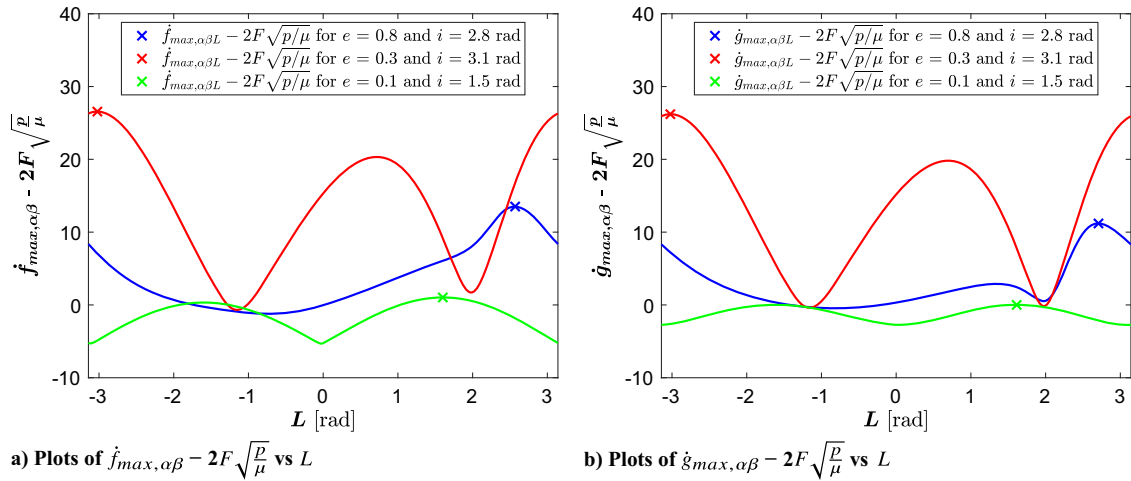


Fig. 3 The correct orbit-dependent values of $\dot{f}_{\max,\alpha\beta L}$ and $\dot{g}_{\max,\alpha\beta L}$ are compared with their approximation, $2F\sqrt{p/\mu}$. The differences $\dot{f}_{\max,\alpha\beta L} - 2F\sqrt{p/\mu}$ and $\dot{g}_{\max,\alpha\beta L} - 2F\sqrt{p/\mu}$, with nondimensionalized units TU^{-1} , are indicated by markers.

All partial derivatives in Eq. (36) have closed-form expressions, except for $\partial \dot{f}_{C,\max,\alpha\beta L} / \partial \alpha_C$ and $\partial \dot{g}_{C,\max,\alpha\beta L} / \partial \alpha_C$. These are enclosed by dashed boxes and must be calculated numerically.

To do this, we evaluate Eqs. (25) and (26), at a mesh of 100 true longitude values in $[0, 2\pi]$ to find the $L_{C,\max,\dot{f}}$ and $L_{C,\max,\dot{g}}$ values that maximize $\dot{f}_{C,\max,\alpha\beta}$ and $\dot{g}_{C,\max,\alpha\beta}$, respectively. It was discovered that $\partial \dot{f}_{C,\max,\alpha\beta} / \partial \alpha_C$ and $\partial \dot{g}_{C,\max,\alpha\beta} / \partial \alpha_C$ also have closed-form expressions, so we use the following approximations:

$$\frac{\partial \dot{f}_{C,\max,\alpha\beta L}}{\partial \alpha_C} \approx \left. \frac{\partial \dot{f}_{C,\max,\alpha\beta}}{\partial \alpha_C} \right|_{L_{C,\max,\dot{f}}} \quad (37)$$

$$\frac{\partial \dot{g}_{C,\max,\alpha\beta L}}{\partial \alpha_C} \approx \left. \frac{\partial \dot{g}_{C,\max,\alpha\beta}}{\partial \alpha_C} \right|_{L_{C,\max,\dot{g}}} \quad (38)$$

We note that Eqs. (37) and (38) are only approximations and not exact relations, since $L_{C,\max,\dot{f}}$ and $L_{C,\max,\dot{g}}$ can depend on α_C . Now that the partial derivatives $\partial \dot{f}_{C,\max,\alpha\beta L} / \partial \alpha_C$ and $\partial \dot{g}_{C,\max,\alpha\beta L} / \partial \alpha_C$, as well as the quantities $L_{C,\max,\dot{f}}$, $L_{C,\max,\dot{g}}$, $\dot{f}_{C,\max,\alpha\beta L}$, and $\dot{g}_{C,\max,\alpha\beta L}$, have been found numerically, Eq. (36) can be evaluated. Furthermore, if we gather terms based on the thrust angles, the following expression for \dot{Q} can be obtained:

$$\dot{Q} = D_1 \cos \beta \cos \alpha + D_2 \cos \beta \sin \alpha + D_3 \sin \beta + \frac{\partial Q}{\partial L_C} b_{C,6} + \frac{\partial Q}{\partial L_T} b_{T,6} \quad (39)$$

where

$$D_1 = \sum_{\alpha} \left(\frac{\partial Q}{\partial \alpha_C} + \frac{\partial Q}{\partial \dot{f}_{C,\max,\alpha\beta L}} \frac{\partial \dot{f}_{C,\max,\alpha\beta L}}{\partial \alpha_C} + \frac{\partial Q}{\partial \dot{g}_{C,\max,\alpha\beta L}} \frac{\partial \dot{g}_{C,\max,\alpha\beta L}}{\partial \alpha_C} \right) \frac{\partial \alpha_C}{\partial F_{\theta}} \quad (40)$$

$$D_2 = \sum_{\alpha} \left(\frac{\partial Q}{\partial \alpha_C} + \frac{\partial Q}{\partial \dot{f}_{C,\max,\alpha\beta L}} \frac{\partial \dot{f}_{C,\max,\alpha\beta L}}{\partial \alpha_C} + \frac{\partial Q}{\partial \dot{g}_{C,\max,\alpha\beta L}} \frac{\partial \dot{g}_{C,\max,\alpha\beta L}}{\partial \alpha_C} \right) \frac{\partial \alpha_C}{\partial F_r} \quad (41)$$

$$D_3 = \sum_{\alpha} \left(\frac{\partial Q}{\partial \alpha_C} + \frac{\partial Q}{\partial \dot{f}_{C,\max,\alpha\beta L}} \frac{\partial \dot{f}_{C,\max,\alpha\beta L}}{\partial \alpha_C} + \frac{\partial Q}{\partial \dot{g}_{C,\max,\alpha\beta L}} \frac{\partial \dot{g}_{C,\max,\alpha\beta L}}{\partial \alpha_C} \right) \frac{\partial \alpha_C}{\partial F_h} + \frac{\partial Q}{\partial L_C} A_{C,(6,3)} \quad (42)$$

For the orbital transfer problem, which does not involve rendezvous, the expressions for D_i were derived by differentiating the original form of $\dot{Q} = D_1 \cos \beta \cos \alpha + D_2 \cos \beta \sin \alpha + D_3 \sin \beta$ with respect to α and β and setting the resulting equations to zero [24,25,38]. Since the derivatives $d(\cdot)/d\alpha$ and $d(\cdot)/d\beta$, of the last two terms in Eq. (39), $(\partial Q / \partial L_C) b_{C,6}$ and $(\partial Q / \partial L_T) b_{T,6}$, are zero, we can express the Lyapunov-optimal thrust angles [24], α^* and β^* , as

$$\alpha^* = \arctan2(-D_2, -D_1) \quad (43)$$

and

$$\beta^* = \arctan\left(\frac{-D_3}{\sqrt{D_1^2 + D_2^2}}\right) \quad (44)$$

where the two-argument arctangent is used for finding α^* and the new expressions for D_i given in Eqs. (40–42) are used. With this alternate formulation, the D_i can be calculated more accurately depending on the resolution of the mesh used for finding $L_{C,\max,\dot{f}}$ and $L_{C,\max,\dot{g}}$.

We note that when evaluating the D_i in Eqs. (40–42), the normalized propulsive acceleration magnitude ($F = 1$) is used, because our goal is to determine expressions for the instantaneous Lyapunov-optimal thrust direction for any given propulsive acceleration. Because F appears simply as a scale factor in the denominator of Q , in Eq. (7), this assumption is also used for the evaluation of Q as well as \dot{Q} , in the calculation of the relative effectivity. However, propagation of the dynamics is done with the correct nondimensionalized value of F .

C. Analysis of Singularities

Because the classical orbital elements have singularities at $i = 0$ rad and $e = 0$, it is expected that formulations of the Q-Law based on classical elements [23,33,39] would not be suitable to analyze orbits close to these singularities. Indeed, Hatten [39], in his implementation of the Q-Law [23], restricted the eccentricity to be greater than a threshold of 5×10^{-3} and the inclination to stay above a threshold of 1×10^{-4} rad. To handle equatorial and more circular orbits, as in the present work, with smaller eccentricities around $e = 0.001$, it was found that modified equinoctial elements need to be used.

The modified equinoctial elements themselves are free of singularities for all orbits other than retrograde equatorial orbits ($i = \pi$ rad), and this singularity can be seen from the $\tan(i/2)$ terms in the definition of the elements h and k in Eqs. (4) and (5), respectively. However, we note that a perfectly circular orbit with $e = 0$ and a parabolic orbit with $e = 1$ cannot be handled by the RQ-Law described in Sec. II.B. Both of these additional singularities arise from the first term of Q in Eq. (7), which contains the factor

$\gamma = (1/\dot{a}_{C,\max,\alpha\beta L})^2$. We note that in the following analysis of the singularities, the subscript C , used to denote association of the orbital elements with the chaser spacecraft, has been dropped in many instances for clarity. The singularity at $e = 1$ exists, since the denominator of γ will be zero whenever $e = \sqrt{f^2 + g^2} = 1$. This is seen from Eq. (9), where we have that

$$\dot{a}_{\max,\alpha\beta L} = 2Fa \sqrt{\frac{a}{\mu}} \sqrt{\frac{1 + \sqrt{f^2 + g^2}}{1 - \sqrt{f^2 + g^2}}}$$

For the second singularity, at $e = 0$, let us first observe that the partial derivative $\partial Q/\partial f$ needs to be evaluated in order to determine \dot{Q} in Eq. (36) and for the D_i in Eqs. (40–42). Because the product rule requires that $\partial\gamma/\partial f$ be evaluated in order to find $\partial Q/\partial f$, we determine that

$$\frac{\partial\gamma}{\partial f} = \frac{-f\mu}{2F^2 a^3 (\sqrt{f^2 + g^2} + 1)^2 \sqrt{f^2 + g^2}} \quad (45)$$

It is seen that $e = \sqrt{f^2 + g^2} = 0$ will cause the denominator of $\partial\gamma/\partial f$ to be zero, which reveals the singularity. In addition, we know from a proof by Gurfil [40] that a parabolic escape trajectory cannot be reached through continuous feedback control. Therefore, the RQ-Law is restricted to orbits with $i \neq \pi$ rad and $0 < e < 1$.

Next, we investigate if these singularities can be avoided by using the semilatus rectum, p , instead of the semimajor axis, a , in the RQ-Law formulation. From Yuan et al. [37], it is stated that

$$\dot{p}_{\max,\alpha\beta} = \frac{2Fp}{1 + f \cos(L) + g \cos(L)} \sqrt{\frac{p}{\mu}}$$

To determine $\dot{p}_{\max,\alpha\beta L}$, we find that

$$\frac{\partial \dot{p}_{\max,\alpha\beta}}{\partial L} = \frac{-2Fp(g \cos(L) - f \sin(L)) \sqrt{p/\mu}}{(f \cos(L) + g \sin(L) + 1)^2} \quad (46)$$

The expression for $\partial \dot{p}_{\max,\alpha\beta}/\partial L$ is zero when $\tan(L) = g/f$ and it is found that $L_{\max,p} = (\arctan2(g, f) + \pi)$ maximizes $\dot{p}_{\max,\alpha\beta}$. After making the substitution $p = a(1 - f^2 - g^2)$, so that the dependence

on f and g can be revealed for analysis, we can write

$$\dot{p}_{\max,\alpha\beta L} = \left(\frac{2Fa(1 - f^2 - g^2)}{1 + f \cos(\arctan2(g, f) + \pi) + g \cos(\arctan2(g, f) + \pi)} \right) \times \sqrt{\frac{a(1 - f^2 - g^2)}{\mu}} \quad (47)$$

A reformulation of the RQ-Law using p instead of a would result in the factor $\xi = (1/\dot{p}_{C,\max,\alpha\beta L})^2$ appearing in the first term of Q . Immediately, it is seen that the singularity at $e = 1$ remains since $e = \sqrt{f^2 + g^2} = 1$ would cause Eq. (47) to be zero. While Eq. (47) is the most general form of $\dot{p}_{\max,\alpha\beta L}$, let us make the restriction $f > 0$ so that $\arctan2(g, f)$ can be replaced by $\arctan(g/f)$ in Eq. (47) and analysis of the second singularity can proceed. From the same reasoning as for γ , since the evaluation of $\partial\xi/\partial f$ would be required in order to find $\partial Q/\partial f$, it is found that

$$\frac{\partial\xi}{\partial f} = \frac{3\mu(f - 2|f|\sqrt{f^2 + g^2} + fg^2 + f^3)}{2F^2 a^3 (f^2 + g^2 - 1)^4} - \frac{\mu|f|(f^2|f| - f\sqrt{f^2 + g^2} + g^2|f|)}{2F^2 a^3 f(f^2 + g^2)(f^2 + g^2 - 1)^3} \quad (48)$$

The denominator of the second term of Eq. (48) contains the factor $(f^2 + g^2)$, which shows that the singularity at $e = \sqrt{f^2 + g^2} = 0$ still exists.

This analysis shows that the RQ-Law has singularities at $i = \pi$, $e = 0$, and $e = 1$. It also suggests that other Q-Law variants that use the semimajor axis, a , or the semilatus rectum, p , in their formulations may not be able to target a perfectly circular orbit either, if the $(1/\dot{\alpha}_{C,\max,\alpha\beta L})^2$ factor appears in the definition of Q . Using the modified equinoctial elements with p replaced by a seems to be the current state-of-the-art for Q-Law formulations as it allows targeting noncircular prograde equatorial orbits, allows targeting eccentricities closer to zero than would be possible through the use of classical elements [39], and offers improved controller performance compared to using the original set of modified equinoctial elements with the semilatus rectum [24].

Table 2 Physical parameters common to all trade studies

m_0 , kg	P_{eng} , kW	η_{eng} , %	I_{sp} , s	g_0 , m/s ²	t_0 , s	μ , m ³ /s ²	R_{Earth} , m	DU , m	TU, S
450	5	65	3300	9.81	0	3.9860×10^{14}	6.3781×10^6	R_{Earth}	$\sqrt{R_{\text{Earth}}^3/\mu}$

Table 3 RQ-law parameters common to all trade studies

Stage	k_{pen}	$r_{p,\text{min}}$	W_p	W_a	W_f	W_g	W_h	W_k	m_{scl}	n_{scl}	r_{scl}	$L_{\text{err,tol}}$ [rad]
1	100	R_{Earth}	1	2	50	50	1	1	3	4	2	N/A
2	100	R_{Earth}	1	10	1	1	1	1	3	4	2	3×10^{-3}

Table 4 Initial classical orbital elements for the chaser and target

Element	Chaser Departure Point Trade Study		Stage Switchover Point Trade Study		Target Orbit Eccentricity Trade Study	
	Chaser	Target	Chaser	Target	Chaser	Target
a [m]	$R_{\text{Earth}} + 2000 \times 10^3$	$R_{\text{Earth}} + 3000 \times 10^3$	$R_{\text{Earth}} + 2000 \times 10^3$	$R_{\text{Earth}} + 3000 \times 10^3$	$R_{\text{Earth}} + 20000 \times 10^3$	$R_{\text{Earth}} + 20000 \times 10^3$
e	0.2	0.001	0.2	0.001	e_T	e_T
i [rad]	0	$\pi/2$	0	$\pi/2$	$\pi/2$	$\pi/2$
ω [rad]	0	$\pi/2$	0	$\pi/2$	$\pi/2$	$\pi/2$
Ω [rad]	—	$\pi/2$	—	$\pi/2$	$\pi/2$	$\pi/2$
θ [rad]	θ_{C0}	$\pi/2$	π	$\pi/2$	0	$\pi/2$

III. Numerical Results and Comparison

In this section, we numerically analyze the RQ-Law described in Sec. II.B through three trade studies and a comparison with existing control laws. The physical parameters used are detailed in Table 2,

and the initial mass and ion thruster characteristics are referenced from a case studied by Kluever and Oleson [41]. Parameters for the RQ-Law were chosen through a combination of problem-specific tuning and reference to prior work [23,33] and the parameters

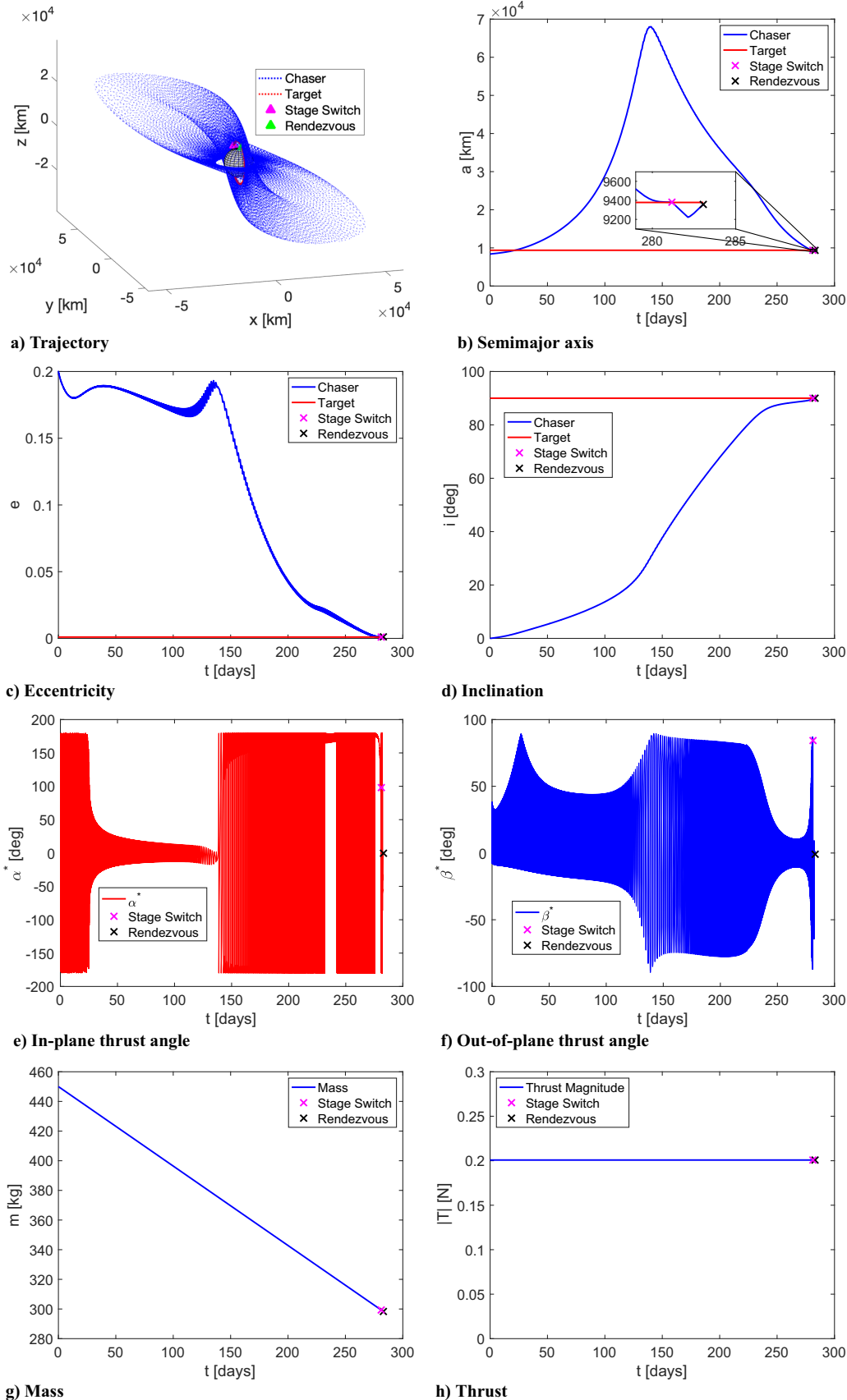


Fig. 4 RQ-Law six-element rendezvous—Chaser Departure Point Trade Study ($\theta_{c0} = 0$).

common to all the cases in this work are provided in Table 3. The ode45 numerical integrator in MATLAB [42] is used with relative and absolute integration tolerances of 1×10^{-9} and 1×10^{-7} , respectively. We emphasize that our approach only assumes two-body Keplerian dynamics with thrusting.

Each analyzed rendezvous trajectory is separated into the orbit acquisition stage (stage 1) and the target acquisition stage (stage 2), as recommended by Naasz in his study of mean motion control [26]. In stage 1, $W_L = 0$ and the chaser's goal is to transfer to the same orbit as the target, matching all the target orbital elements except for L_T . Stage 1 termination is determined by a tolerance in Q , denoted by Q_{tol} . For stage 2, $W_L > 0$ and the chaser will try to match the true longitude of the moving target in order to achieve rendezvous. If coasting is enabled through $\eta_{r,tol} > 0$, it is performed only in stage 1, as it has been found to interfere with the phasing maneuvers in stage 2, resulting in missed rendezvous opportunities and increased fuel consumption. The phasing parameters W_L and W_{sc1} and the tolerances $\eta_{r,tol}$ and Q_{tol} are discussed separately for each trade study. We note that Q_{tol} is given without units because nondimensionalized time is used internally for the RQ-Law. The termination condition for stage 2 is such that the true longitude errors are less than 3×10^{-3} rad for all of the rendezvous cases studied in this work.

A. Chaser Departure Point Trade Study

The first trade study analyzes the effect of the departure point of the chaser on the performance of the RQ-Law. The rationale for this study

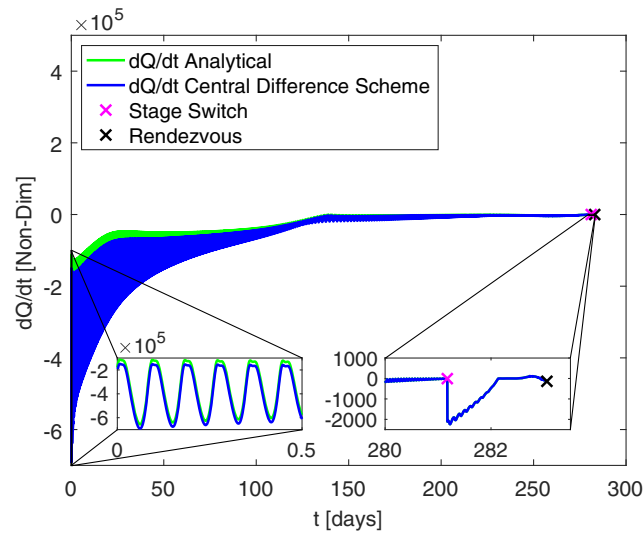


Fig. 5 Comparison of analytical \dot{Q} history computed from Eq. (36) with numerically differentiated Q history—Chaser Departure Point Trade Study ($\theta_{C0} = 0$).

is to see whether it would make a significant difference in performance to wait until a favorable relative geometry between the chaser and target is reached, before initiating the rendezvous trajectory. The rendezvous trajectories generated for this study involve significant changes in all six orbital elements. In Table 4, the initial orbital elements for the chaser and target are given under the subheading for the chaser departure point trade study, where it is indicated that the initial chaser true anomaly, θ_{C0} , is varied. The tolerances $Q_{tol} = 1 \times 10^{-7}$ and $\eta_{r,tol} = 0$ were used, which shows that coasting is not considered in this trade study. The phasing parameters $W_L = 0.06609$ and $W_{sc1} = 3.3697$ are used for all cases in this trade study and were tuned through the *fminsearch* Nelder–Mead optimization routine in MATLAB, by minimizing the stage 2 fuel consumption for the $\theta_{C0} = 0$ case. Because the target orbital elements are the same for all cases in this trade study, good performance was found in using the phasing parameters optimized specifically for the $\theta_{C0} = 0$ case, for all cases. Figure 4 shows the trajectory, the time histories of the critical orbital elements, the thrust angles, as well as the mass and thrust histories for the rendezvous trajectory corresponding to $\theta_{C0} = 0$. It is seen that the target elements are reached and it is interesting to note that in Fig. 4b, the RQ-Law inherits a characteristic property of the Q-Law where the semimajor axis is temporarily increased past the desired value in order to more efficiently change the inclination and the right ascension of the ascending node (RAAN) by increasing their maximal rates of change [39]. In addition, the inset in Fig. 4b shows the effect of the semimajor axis augmentation scheme introduced in Eq. (8) and Fig. 1 that allows the rendezvous to occur. Classical elements are used for clarity in Table 4 and Fig. 4, even though the numerical integration is done using modified equinoctial elements.

The case of $\theta_{C0} = 0$ in this trade study was also taken as an opportunity to numerically validate the expression for \dot{Q} in Eq. (36), as it is critical to the RQ-Law formulation. In Fig. 5, a plot of \dot{Q} computed analytically through Eq. (36) is compared with a plot of the numerically differentiated time history of Q , computed through a central difference scheme. As stated at the end of Sec. II.B.1, since $F = 1$ is assumed when calculating Q , it is actually the time history of Q/F^2 that must be used when calculating \dot{Q} through finite differencing. The plot insets show that although there is a minor discrepancy, the shape of the plots shows good agreement. We believe that this difference can be attributed to our use of grid-searched values in the approximations in Eqs. (37) and (38). In addition, the difference diminishes over time, and this is especially apparent in the inset comparing the plots at the end of the trajectory.

To evaluate its performance in this trade study, the RQ-Law is compared with a hybrid comparison control scheme that uses the Varga and Pérez Q-Law [24] for the orbital transfer in stage 1 and a simple tangential thrust spiral phasing law for stage 2 that is described by King et al. [36]. The tangential phasing law causes the chaser to initially spiral up or down, depending on whether the

Table 5 Fuel consumption and transfer time breakdown by stage for the chaser departure point trade study for the RQ-law (RQ) and Varga and Pérez Q-law with tangential thrust spiral phasing (VP+T)

	$\theta_{C0} = 0$				$\theta_{C0} = \pi/4$				$\theta_{C0} = \pi/2$				$\theta_{C0} = 3\pi/4$			
	Δm , kg		Δt , days		Δm , kg		Δt , days		Δm , kg		Δt , days		Δm , kg		Δt , days	
	RQ	VP + T	RQ	VP + T	RQ	VP + T	RQ	VP + T	RQ	VP + T	RQ	VP + T	RQ	VP + T	RQ	VP + T
Stage 1	150.67	151.29	281.17	282.32	150.67	151.28	281.17	282.31	150.67	151.28	281.17	282.31	150.67	151.28	281.16	282.3
Stage 2	1.01	0.59	1.88	1.1	1.15	0.44	2.15	0.82	0.84	0.4	1.57	0.75	0.66	0.41	1.23	0.77
Total	151.68	151.88	283.06	283.42	151.82	151.72	283.32	283.13	151.51	151.68	282.73	283.06	151.33	151.69	282.39	283.07
	$\theta_{C0} = \pi$				$\theta_{C0} = 5\pi/4$				$\theta_{C0} = 3\pi/2$				$\theta_{C0} = 7\pi/4$			
	Δm , kg		Δt , days		Δm , kg		Δt , days		Δm , kg		Δt , days		Δm , kg		Δt , days	
	RQ	VP + T	RQ	VP + T	RQ	VP + T	RQ	VP + T	RQ	VP + T	RQ	VP + T	RQ	VP + T	RQ	VP + T
Stage 1	150.67	151.29	281.16	282.32	150.67	151.28	281.17	282.31	150.67	151.29	281.18	282.33	150.68	151.29	281.18	282.32
Stage 2	0.73	0.99	1.36	1.85	1.26	1.46	2.36	2.72	1.63	1.19	3.04	2.23	1.25	0.88	2.33	1.64
Total	151.4	152.28	282.52	284.17	151.93	152.74	283.52	285.03	152.3	152.48	284.22	284.55	151.92	152.17	283.51	283.96

chaser is ahead or behind the target, respectively, until half the phase angle difference is covered, at which point the spiral maneuver is reversed until rendezvous is achieved. This simple tangential phasing law, with equal phase difference coverage in the spiral up and spiral down arcs, is applicable for near-circular orbits. This is valid for this trade study since $e_T = 0.001$. We note that the parameters in Tables 2 and 3 are also used for the stated hybrid comparison law. The results of this chaser departure point trade study are shown in

Table 5 and Fig. 6. From Table 5, it is apparent that for both laws the chaser departure point affects the stage 2 fuel consumption but has a negligible impact for stage 1. This is expected because changing the departure point of the chaser will change the phase difference at the beginning of stage 2. However in stage 1, only the slow orbital elements are targeted. In general, the RQ-Law offers better performance in stage 1 compared to the Varga and Pérez Q-Law, due to the alternate method of thrust angle determination presented in

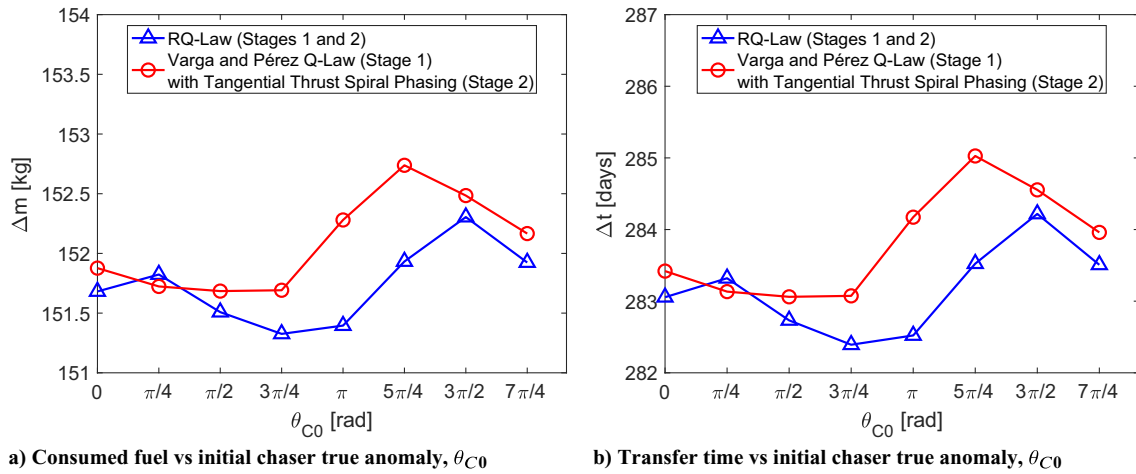


Fig. 6 Comparison of the RQ-Law with the Varga and Pérez Q-Law [24] with tangential phasing [36]—Chaser Departure Point Trade Study.

Table 6 Fuel consumption and transfer time breakdown by stage for the Stage Switchover Point Trade Study for the RQ-Law (RQ) and Varga and Pérez Q-Law with tangential thrust spiral phasing (VP + T)

	$Q_{tol} = 1 \times 10^{-7}$				$Q_{tol} = 1 \times 10^{-6}$				$Q_{tol} = 1 \times 10^{-5}$				$Q_{tol} = 1 \times 10^{-4}$			
	Δm , kg		Δt , days		Δm , kg		Δt , days		Δm , kg		Δt , days		Δm , kg		Δt , days	
	RQ	VP + T	RQ	VP + T	RQ	VP + T	RQ	VP + T	RQ	VP + T	RQ	VP + T	RQ	VP + T	RQ	VP + T
Stage 1	141.64	141.86	320.26	320.83	141.57	141.79	320.09	320.66	141.34	141.56	319.61	320.15	140.77	140.97	318.44	318.93
Stage 2	1.54	1.19	2.87	2.21	1.55	1.19	2.89	2.22	1.6	---	2.99	---	2.27	---	4.24	---
Total	143.18	143.05	323.12	323.04	143.12	142.98	322.98	322.88	142.95	---	322.6	---	143.04	---	322.68	---
	$Q_{tol} = 1 \times 10^{-3}$				$Q_{tol} = 1 \times 10^{-2}$				$Q_{tol} = 1 \times 10^{-1}$				$Q_{tol} = 1 \times 10^0$			
	Δm , kg		Δt , days		Δm , kg		Δt , days		Δm , kg		Δt , days		Δm , kg		Δt , days	
	RQ	VP + T	RQ	VP + T	RQ	VP + T	RQ	VP + T	RQ	VP + T	RQ	VP + T	RQ	VP + T	RQ	VP + T
Stage 1	139.42	139.6	315.93	316.38	134.81	134.99	307.28	307.73	97.3	97.58	231.51	233.34	34.59	34.98	87.85	90.12
Stage 2	3.46	---	6.46	---	8.06	---	15.05	---	---	---	---	---	---	---	---	---
Total	142.88	---	322.39	---	142.88	---	322.33	---	---	---	---	---	---	---	---	---

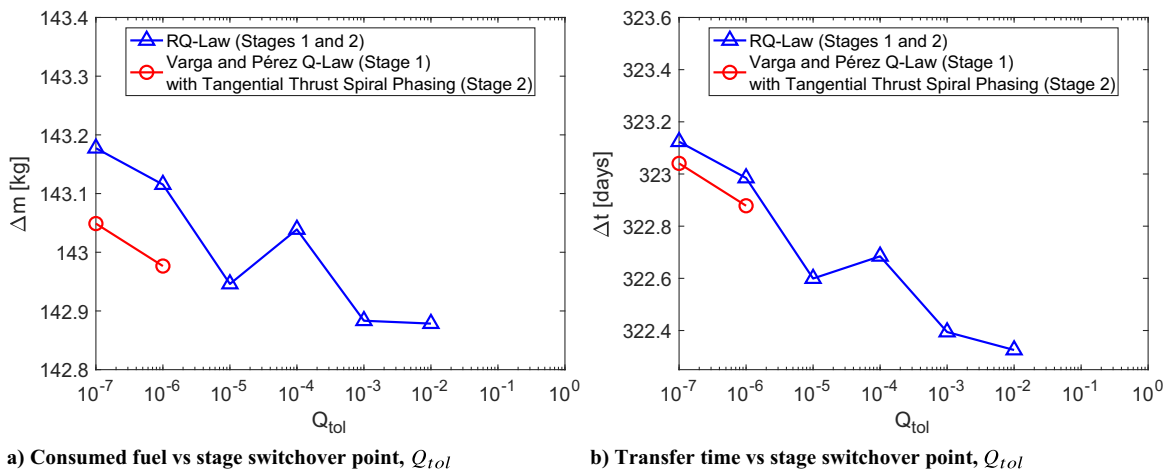


Fig. 7 Comparison of the RQ-Law with the Varga and Pérez Q-Law [24] with tangential phasing [36]—Stage Switchover Point Trade Study.

Sec. II.B.1, while the phasing maneuver in stage 2 is more efficiently done by the simple tangential spiral maneuver for the near-circular case. As seen in Table 5 and Fig. 6, the trends found from the comparison of the fuel consumption breakdown by stage also

hold for the transfer time. We see that for all but one of the cases considered, the RQ-Law offers slightly improved performance with respect to the comparison law, in terms of both fuel consumption and transfer time.

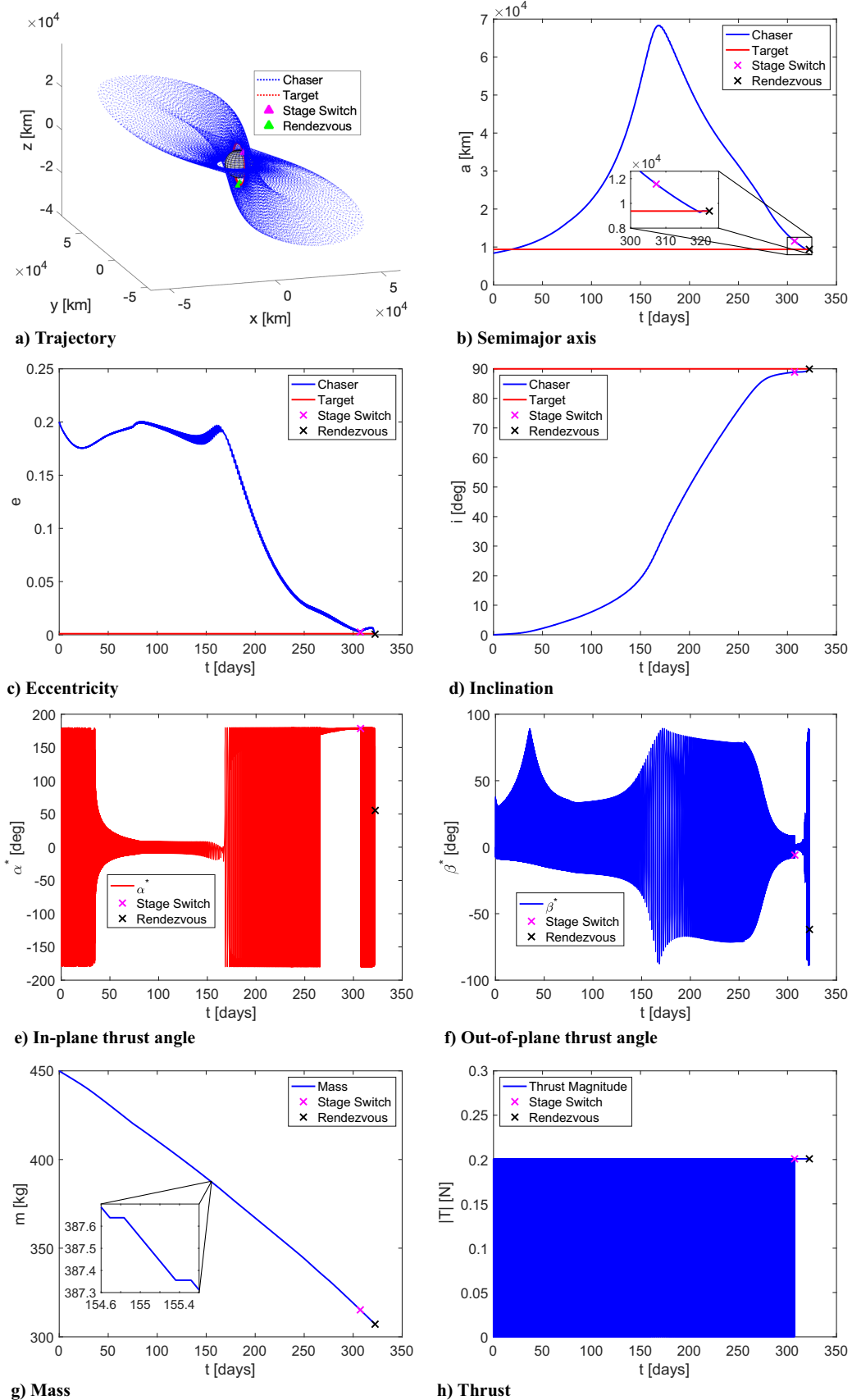


Fig. 8 RQ-Law six-element rendezvous—Stage Switchover Point Trade Study ($Q_{tot} = 1 \times 10^{-2}$).

B. Stage Switchover Point Trade Study

The second trade study investigates whether the RQ-Law performance is affected by the choice of Q_{tol} —that is, whether starting the target acquisition in stage 2 earlier in the trajectory results in improved performance. From Table 4, it is seen that the initial orbital elements for this trade study correspond to the elements for the chaser departure point trade study with $\theta_{C0} = \pi$. The same phasing parameters as in the previous trade study, $W_L = 0.06609$ and $W_{\text{scl}} = 3.3697$, are used. Coasting is enabled through the use of $\eta_{r,\text{tol}} = 0.1$. The results are presented in Table 6 and visualized in Fig. 7. For the case corresponding to $Q_{\text{tol}} = 1 \times 10^{-7}$, we are able to directly see the effect of coasting by comparing with the $\theta_{C0} = \pi$ case in Table 5. For the RQ-Law, noticeable fuel savings of about 8 kg are observed at the cost of approximately an extra 40 days in transfer time. To study the effect of Q_{tol} , it has been found that for all of the cases, stage 1 converges, but as Q_{tol} increases, problems with rendezvous in stage 2 start occurring for both the RQ-Law and the comparison law. For the purpose of this investigation, when the total fuel consumption reaches 170 kg, nonconvergence is declared and the corresponding case in Table 6 is marked with a dash, and the corresponding data are removed in Fig. 7. It is seen that the RQ-Law converges up to $Q_{\text{tol}} = 1 \times 10^{-2}$ while the comparison law is only able to converge up to $Q_{\text{tol}} = 1 \times 10^{-6}$. Although the RQ-Law outperforms the comparison for all cases in stage 1, the hybrid comparison law outperforms the RQ-Law due to better stage 2 performance, when it is able to converge. We emphasize that, for the hybrid comparison law, the convergence problems are not associated with the Varga and Pérez Q-Law associated with stage 1, but rather with the tangential thrust spiral phasing law in stage 2. However, as Q_{tol} increases, performance improves overall, and at $Q_{\text{tol}} = 1 \times 10^{-2}$, the RQ-Law is able to offer better performance than the best possible performance by the hybrid comparison law at $Q_{\text{tol}} = 1 \times 10^{-6}$, as seen in Fig. 7. This case can be more closely observed in Fig. 8. In Figs. 8g and 8h, the effect of coasting is clearly seen, where one can observe the plateaus in the mass history and the rapid switching of the thrust magnitude up to the end of stage 1.

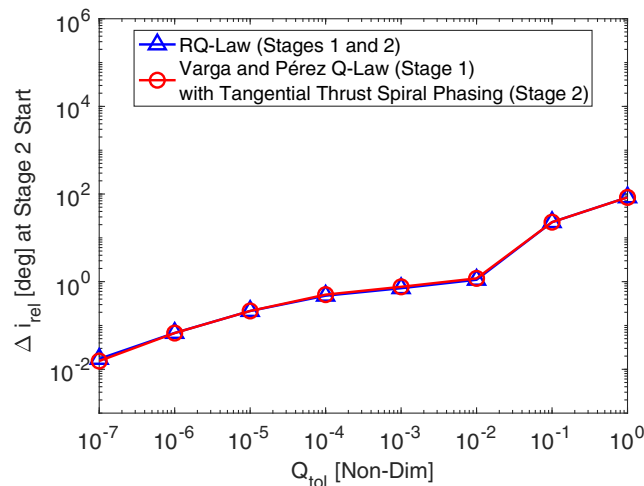


Fig. 9 Relative inclination at stage 2 start vs stage switchover point—Stage Switchover Point Trade Study.

It has been stated by Izzo et al. [43], that the relative inclination,

$$\Delta i_{\text{rel}} = \cos^{-1}(\cos i_1 \cos i_2 + \sin i_1 \sin i_2 \cos \Omega_1 \cos \Omega_2 + \sin i_1 \sin i_2 \sin \Omega_1 \sin \Omega_2) \quad (49)$$

between two orbits is a good measure of the orbital transfer cost between them. Therefore, we use the relative inclination as a metric to characterize the distance between the osculating orbit of the chaser and the target orbit at the start of stage 2. The results are given in Fig. 9, and it is seen that, approximately, the RQ-Law stage 2 is able to converge for $\Delta i_{\text{rel}} \leq 1$ deg, while the tangential thrust spiral phasing law in the comparison is able to converge for $\Delta i_{\text{rel}} \leq 0.07$ deg. The results of this trade study show that, in general, a two-stage approach, with a sufficiently small Q_{tol} , is necessary for the RQ-Law.

C. Target Orbit Eccentricity Trade Study

The third trade study analyzes the phasing performance of the RQ-Law for generating rendezvous trajectories to targets in orbits with various eccentricities. The rationale for this trade study is to see whether the RQ-Law can perform rendezvous in eccentric target orbits, which is a more difficult task than rendezvous in circular orbits. A value of $Q_{\text{tol}} = 1 \times 10^{-7}$ is used and because the chaser starts on the desired orbit but is initially separated from the target by a phase difference of $\pi/2$ rad, this study happens entirely in stage 2 as $Q(t=0) \leq Q_{\text{tol}}$ for all cases. Therefore, this study highlights the target semimajor axis augmentation scheme presented in Eq. (8) and Fig. 1. As mentioned earlier, $\eta_{r,\text{tol}} = 0$ since coasting is disabled in stage 2. The initial orbital elements used for this trade study are given in Table 4, where it is indicated that the target eccentricity, e_T , is varied. For this trade study, because different eccentricities are targeted, different phasing parameters are used for each case and are found using the Nelder–Mead implementation in *fminsearch*. In this optimization, the phasing parameters that minimized the fuel consumption for each of the e_T cases were found. These parameters are given in Table 7. The results of this study are given in Figs. 10 and 11. In Fig. 10b, the effect of the semimajor axis augmentation scheme is clearly seen, where the value of a is temporarily reduced to $a_{T,\text{aug}}$, in order to perform phasing. It is seen that, without a significant variation in fuel consumption and transfer time, the RQ-Law is able to perform phasing in a range of orbits, from near-circular ($e = 0.001$) to moderately high eccentricity ($e = 0.7$).

D. Note on Parameter Selection

It has been found in our investigations that the parameters in Table 3 work well for geocentric orbits. The k_{pen} and W_p parameters were adopted from Lantukh et al. [33] and the m_{scl} , n_{scl} , and r_{scl} parameters were adopted from Petropoulos [23]. We note that, for the penalties, the absolute values are not so important as are their relative magnitudes. To that effect, in stage 1, W_f and W_g are made larger than the other penalties to prevent the eccentricity from growing too large and going near the singularity at $e = 1$. However, for a rendezvous case that only requires orbit raising, W_a can be made larger than the other parameters. In stage 2, the emphasis is on reducing the phasing error and this is done indirectly by choosing a larger value of W_a , so that the chaser semimajor axis tracks the augmented value of the target semimajor axis, according to Eq. (8). The value of Q_{tol} is chosen to be as large as possible in order to allow rendezvous in stage 2, and it has been found that $Q_{\text{tol}} = 1 \times 10^{-7}$ is a good initial

Table 7 RQ-law phasing parameters for target eccentricity trade study

Parameter	$e_T = 0.001$	$e_T = 0.1$	$e_T = 0.2$	$e_T = 0.3$	$e_T = 0.4$	$e_T = 0.5$	$e_T = 0.6$	$e_T = 0.7$
W_L	0.0594	0.0621	0.0661	0.0548	0.0702	0.1123	0.0661	0.0659
W_{scl}	3.6230	3.6952	3.3714	5.4849	3.6663	1.9891	3.5557	3.2053

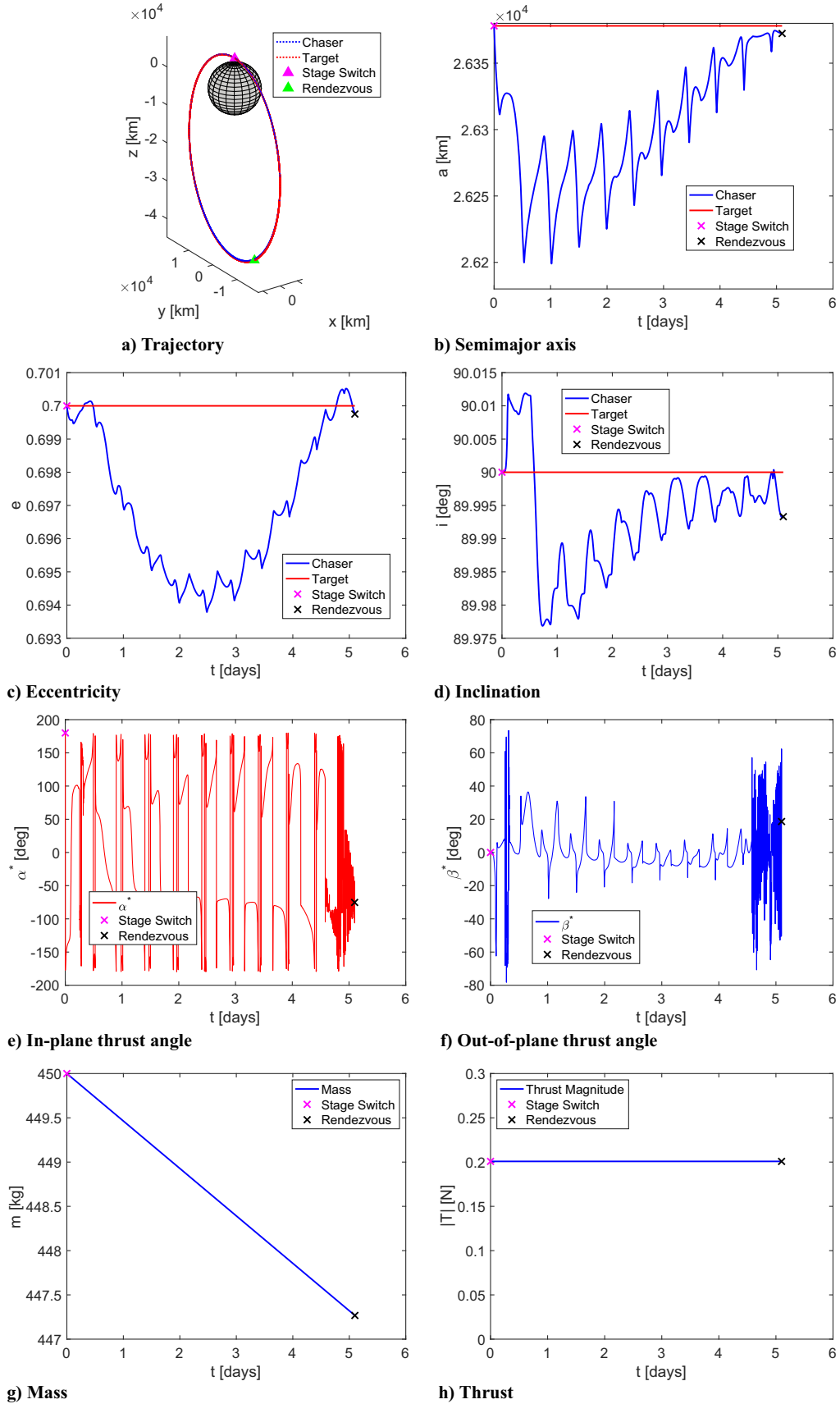


Fig. 10 RQ-Law phasing—Target Orbit Eccentricity Trade Study ($e_T = 0.7$).

value to try. The phasing parameters W_{sc1} and W_L are typically tuned through trial and error to achieve rendezvous. These two parameters can then be optimized, if needed, by approaches such as the derivative-free Nelder–Mead optimization method, as shown in this

work. For geocentric orbits, the values $W_{sc1} = 0.7$ and $W_L = 0.06$ were found to be good starting points for an initial trial and error search. After these parameters are found, a nonzero value of $\eta_{r,101}$ can be chosen for stage 1, such that a desired balance between fuel

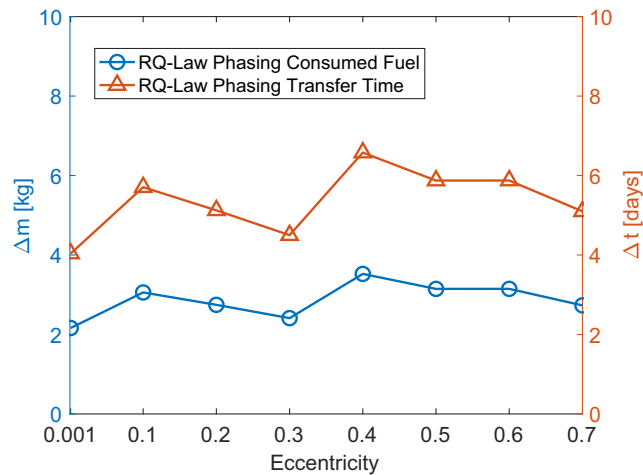


Fig. 11 Transfer time and consumed fuel vs target eccentricity—Target Orbit Eccentricity Trade Study.

consumption and transfer time is achieved. We note that parameter tuning was not a focus of this work, but many excellent studies exist in the literature where a parameter optimizer is wrapped around the Q-Law [24,44]. It is anticipated that such an approach may offer substantial improvements in performance when applied to the RQ-Law.

IV. Conclusions

In this work, the well-known Q-Law, which is a Lyapunov feedback control law for orbital transfers, is adapted to create the RQ-Law for generating low-thrust three-dimensional multirevolution long-range rendezvous trajectories with a moving target based on modified equinoctial elements. The RQ-Law introduces new features for both the orbit and target acquisition stages. In addition to a qualitative comparison of the RQ-Law with other low-thrust Lyapunov feedback control laws from the literature, a numerical comparison of the RQ-Law is performed with a law that combines the Varga and Pérez Q-Law for orbital transfer and a simple tangential thrust spiral scheme for phasing. A detailed singularity analysis for the RQ-Law has been presented, and a discussion of the singularities for similar Q-Law formulations has also been included. The analysis shows that the current state-of-the-art for Q-Law formulations is to use modified equinoctial elements with the semilatus rectum, p , replaced with the semimajor axis, a . Due to the alternate approach of thrust angle determination, it is seen that the RQ-Law offers improved performance in terms of both transfer time as well as consumed fuel. The target semimajor axis augmentation scheme also enables target acquisition in orbits with a range of eccentricities. The trade studies performed show that the performance is influenced by the departure point of the chaser, and the point at which target acquisition is begun, but that the target orbit eccentricity does not have a significant impact. Future work can investigate the effect of eclipsing as well as other perturbative effects, such as nonsphericity of the primary gravitational body. It is seen that the RQ-Law provides a method of quickly generating low-thrust rendezvous trajectories for preliminary design without requiring an initial guess. The resulting trajectory can then be refined with higher-fidelity tools based upon the indirect or direct methods and augmented with a linearized control law for terminal rendezvous.

Acknowledgments

The authors would like to thank Graham Mackintosh of NASA FDL for creating the AI Challenge for Orbital Debris Remediation, which motivated our research into this topic. The authors are grateful to Chit Hong Yam of ispace Inc., and Stefano Campagnola of NASA JPL, who first suggested we look into the Q-Law literature. The authors also thank Dario Izzo of ESA ACT, Luís F. Simões of ML Analytics, Michael Saunders of Stanford University, and Philip Gill

of University of California, San Diego, for valuable discussions. The authors would like to acknowledge the use of the Niagara supercomputer at the University of Toronto and are grateful for support by the Ontario Graduate Scholarship. Finally, the authors thank the anonymous reviewers for their insightful comments and suggestions, which were very helpful.

References

- [1] De Ruiter, A. H. J., Damaren, C. J., and Forbes, J. R., *Spacecraft Dynamics and Control: An Introduction*, Wiley, Chichester, England, U.K., 2013, pp. 65–128.
- [2] Hakima, H., Bazzocchi, M. C. F., and Emami, M. R., “A Deorbiting CubeSat for Active Orbital Debris Removal,” *Advances in Space Research*, Vol. 61, No. 9, 2018, pp. 2377–2392. <https://doi.org/10.1016/j.asr.2018.02.021>
- [3] Bucci, L., and Lavagna, M. R., “Analytical Formulation for Light and Fast Low-Thrust Guidance Design to Perform Multi-Target On-Orbit Servicing,” *AIAA Guidance, Navigation, and Control Conference*, AIAA Paper 2016-0877, 2016. <https://doi.org/10.2514/6.2016-0877>
- [4] Guelman, M., and Aleshin, M., “Optimal Bounded Low-Thrust Rendezvous with Fixed Terminal-Approach Direction,” *Journal of Guidance, Control, and Dynamics*, Vol. 24, No. 2, 2001, pp. 378–385. <https://doi.org/10.2514/2.4722>
- [5] Kumar, Yajur, “Optimal Low Thrust Transfer for Relative Orbital Motion,” M.Tech. Thesis, Indian Institute of Technology, Kanpur, India, 2016.
- [6] Luo, Y., Zhang, J., and Tang, G., “Survey of Orbital Dynamics and Control of Space Rendezvous,” *Chinese Journal of Aeronautics*, Vol. 27, No. 1, 2014, pp. 1–11. <https://doi.org/10.1016/j.cja.2013.07.042>
- [7] Kluever, C. A., and Tanck, G. S., “A Feedback Guidance Scheme for Orbital Rendezvous,” *Journal of the Astronautical Sciences*, Vol. 47, Nos. 3–4, 1999, pp. 229–237. <https://doi.org/10.1007/BF03546201>
- [8] Kechichian, J. A., “Optimal Low-Thrust Rendezvous Using Equinoctial Orbit Elements,” *Acta Astronautica*, Vol. 38, No. 1, 1996, pp. 1–14. [https://doi.org/10.1016/0094-5765\(95\)00121-2](https://doi.org/10.1016/0094-5765(95)00121-2)
- [9] Olympio, J., and Frouvelle, N., “Space Debris Selection and Optimal Guidance for Removal in the SSO with Low-Thrust Propulsion,” *Acta Astronautica*, Vol. 99, June 2014, pp. 263–275. <https://doi.org/10.1016/j.actaastro.2014.03.005>
- [10] Haberkorn, T., Martinon, P., and Gergaud, J., “Low Thrust Minimum-Fuel Orbital Transfer: A Homotopic Approach,” *Journal of Guidance, Control, and Dynamics*, Vol. 27, No. 6, 2004, pp. 1046–1060. <https://doi.org/10.2514/1.4022>
- [11] Sims, J., Finlayson, P., Rinderle, E., Vavrina, M., and Kowalkowski, T., “Implementation of a Low-Thrust Trajectory Optimization Algorithm for Preliminary Design,” AIAA Paper 2006-6746, 2006. <https://doi.org/10.2514/6.2006-6746>
- [12] Yam, C. H., Lorenzo, D. D., and Izzo, D., “Low-Thrust Trajectory Design as a Constrained Global Optimization Problem,” *Proceedings of the Institution of Mechanical Engineers, Part G: Journal of Aerospace Engineering*, Vol. 225, No. 11, 2011, pp. 1243–1251. <https://doi.org/10.1177/0954410011401686>
- [13] Novak, D. M., and Vasile, M., “Improved Shaping Approach to the Preliminary Design of Low-Thrust Trajectories,” *Journal of Guidance, Control, and Dynamics*, Vol. 34, No. 1, 2011, pp. 128–147. <https://doi.org/10.2514/1.50434>
- [14] Petropoulos, A. E., and Longuski, J. M., “Shape-Based Algorithm for the Automated Design of Low-Thrust, Gravity Assist Trajectories,” *Journal of Spacecraft and Rockets*, Vol. 41, No. 5, 2004, pp. 787–796. <https://doi.org/10.2514/1.13095>
- [15] Wall, B. J., and Conway, B. A., “Shape-Based Approach to Low-Thrust Rendezvous Trajectory Design,” *Journal of Guidance, Control, and Dynamics*, Vol. 32, No. 1, 2009, pp. 95–101. <https://doi.org/10.2514/1.36848>
- [16] Taheri, E., Kolmanovsky, I., and Atkins, E., “Shaping Low-Thrust Trajectories with Thrust-Handling Feature,” *Advances in Space Research*, Vol. 61, No. 3, 2018, pp. 879–890. <https://doi.org/10.1016/j.asr.2017.11.006>
- [17] Narayanaswamy, S., and Damaren, C. J., “Comparison of the Legendre–Gauss Pseudospectral and Hermite–Legendre–Gauss–Lobatto Methods for Low-Thrust Spacecraft Trajectory Optimization,” *Aerospace Systems*, Vol. 3, No. 1, 2020, pp. 53–70. <https://doi.org/10.1007/s42401-019-00042-w>

- [18] Graham, K. F., and Rao, A. V., "Minimum-Time Trajectory Optimization of Multiple Revolution Low-Thrust Earth-Orbit Transfers," *Journal of Spacecraft and Rockets*, Vol. 52, No. 3, 2015, pp. 711–727. <https://doi.org/10.2514/1.A33187>
- [19] Kluever, C. A., "Simple Guidance Scheme for Low-Thrust Orbit Transfers," *Journal of Guidance, Control, and Dynamics*, Vol. 21, No. 6, 1998, pp. 1015–1017. <https://doi.org/10.2514/2.4344>
- [20] Ruggiero, A., Pergola, P., Marcuccio, S., and Andrenucci, M., "Low-Thrust Maneuvers for the Efficient Correction of Orbital Elements," *32nd International Electric Propulsion Conference*, Electric Rocket Propulsion Society, Ohio, 2011, pp. 11–15.
- [21] Ilgen, M. R., "Low Thrust OTV Guidance Using Liapunov Optimal Feedback Control Techniques," *Advances in the Astronautical Sciences*, Vol. 85, AAS Paper 93-680, 1993, pp. 1527–1546.
- [22] Ghosh, P., "A Survey of the Methods Available for the Design of Many-Revolution Low-Thrust Planetocentric Trajectories," *Advances in the Astronautical Sciences*, Vol. 168, AAS Paper 19-297, 2019, pp. 395–414.
- [23] Petropoulos, A. E., "Refinements to the Q-Law for Low-Thrust Orbit Transfers," *Advances in the Astronautical Sciences*, Vol. 120, AAS Paper 05-162, 2005, pp. 963–982.
- [24] Varga, G. I., and Pérez, J. M. S., "Many-Revolution Low-Thrust Orbit Transfer Computation Using Equinoctial Q-Law Including J2 and Eclipse Effects," *Advances in the Astronautical Sciences*, Vol. 156, AAS Paper 15-590, 2016, pp. 2463–2481.
- [25] Shannon, J. L., Ozimek, M. T., Atchison, J. A., and Hartzell, C. M., "Q-Law Aided Direct Trajectory Optimization of Many-Revolution Low-Thrust Transfers," *Journal of Spacecraft and Rockets*, Vol. 57, No. 4, 2020, pp. 672–682. <https://doi.org/10.2514/1.A34586>
- [26] Naasz, B. J., "Classical Element Feedback Control for Spacecraft Orbital Maneuvers," M.S. Thesis, Virginia Tech, Blacksburg, VA, May 2002.
- [27] Hernandez, S., and Akella, M. R., "Lyapunov-Based Guidance for Orbit Transfers and Rendezvous in Levi-Civita Coordinates," *Journal of Guidance, Control, and Dynamics*, Vol. 37, No. 4, 2014, pp. 1170–1181. <https://doi.org/10.2514/1.62305>
- [28] Leomanni, M., Bianchini, G., Garulli, A., and Giannitrapani, A., "Non-linear Orbit Control with Longitude Tracking," *2016 IEEE 55th Conference on Decision and Control (CDC)*, Inst. of Electrical and Electronics Engineers, New York, 2016, pp. 1316–1321. <https://doi.org/10.1109/CDC.2016.7798448>
- [29] Petropoulos, A. E., "Simple Control Laws for Low-Thrust Orbit Transfers," *Advances in the Astronautical Sciences*, Vol. 116, AAS Paper 03-630, 2003, pp. 2031–2048.
- [30] Petropoulos, A., "Low-Thrust Orbit Transfers Using Candidate Lyapunov Functions with a Mechanism for Coasting," *AIAA/AAS Astrodynamics Specialist Conference and Exhibit*, AIAA Paper 2004-5089, 2004. <https://doi.org/10.2514/6.2004-5089>
- [31] Joseph, B. E., "Lyapunov Feedback Control in Equinoctial Elements Applied to Low Thrust Control of Elliptical Orbit Constellations," M.S. Thesis, Massachusetts Inst. of Technology, Cambridge, MA, 2006.
- [32] Niccolai, L., Quarta, A. A., and Mengali, G., "Solar Sail Helio-centric Transfers with a Q-law," *Acta Astronautica*, Vol. 188, Nov. 2021, pp. 352–361. <https://doi.org/10.1016/j.actaastro.2021.07.037>
- [33] Lantukh, D. V., Ranieri, C. L., DiPrinzio, M. D., and Edelman, P. J., "Enhanced Q-Law Lyapunov Control for Low-Thrust Transfer and Rendezvous Design," *Advances in the Astronautical Sciences*, Vol. 162, AAS Paper 17-589, 2017, pp. 2741–2752.
- [34] Chang, D. E., Chichka, D. F., and Marsden, J. E., "Lyapunov-Based Transfer between Elliptic Keplerian Orbits," *Discrete & Continuous Dynamical Systems-B*, Vol. 2, No. 1, 2002, p. 57. <https://doi.org/10.3934/dcdsb.2002.2.57>
- [35] Walker, M., Ireland, B., and Owens, J., "A Set of Modified Equinoctial Orbit Elements," *Celestial Mechanics*, Vol. 36, No. 4, 1985, pp. 409–419. <https://doi.org/10.1007/BF01227493>
- [36] King, S., Walker, M., and Kluever, C., "Small Satellite LEO Maneuvers with Low-Power Electric Propulsion," *44th AIAA/ASME/SAE/ASEE Joint Propulsion Conference and Exhibit*, AIAA Paper 2008-4516, 2008. <https://doi.org/10.2514/6.2008-4516>
- [37] Yuan, R., Pingyuan, C., and Enjie, L., "A Low-thrust Guidance Law Based on Lyapunov Feedback Control and Hybrid Genetic Algorithm," *Aircraft Engineering and Aerospace Technology*, Vol. 79, No. 2, 2007, pp. 144–149. <https://doi.org/10.1108/00022660710732699>
- [38] Shannon, J. L., Ellison, D., and Hartzell, C. M., "Analytical Partial Derivatives of the Q-Law Guidance Algorithm," *Advances in the Astronautical Sciences*, Vol. 176, AAS Paper 21-274, 2021.
- [39] Hatten, N. A., "A Critical Evaluation of Modern Low-Thrust, Feedback-Driven Spacecraft Control Laws," M.S. Thesis, Univ. of Texas, Austin, TX, Dec. 2012.
- [40] Gurfil, P., "Nonlinear Feedback Control of Low-Thrust Orbital Transfer in a Central Gravitational Field," *Acta Astronautica*, Vol. 60, Nos. 8–9, 2007, pp. 631–648. <https://doi.org/10.1016/j.actaastro.2006.10.001>
- [41] Kluever, C. A., and Oleson, S. R., "Direct Approach for Computing Near-Optimal Low-Thrust Earth-Orbit Transfers," *Journal of Spacecraft and Rockets*, Vol. 35, No. 4, 1998, pp. 509–515. <https://doi.org/10.2514/2.3360>
- [42] Shampine, L. F., and Reichelt, M. W., "The MATLAB ODE Suite," *SIAM Journal on Scientific Computing*, Vol. 18, No. 1, 1997, pp. 1–22. <https://doi.org/10.1137/S1064827594276424>
- [43] Izzo, D., Getzner, I., Hennes, D., and Simões, L. F., "Evolving Solutions to TSP Variants for Active Space Debris Removal," *Proceedings of the 2015 Genetic and Evolutionary Computation Conference—GECCO '15*, ACM Press, New York, 2015, pp. 1207–1214. <https://doi.org/10.1145/2739480.2754727>
- [44] Petropoulos, A. E., and Lee, S., "Optimisation of Low-Thrust Orbit Transfers Using the Q-law for the Initial Guess," *Advances in the Astronautical Sciences*, Vol. 123, AAS Paper 05-392, 2005.